Supporting information

Ultralow thermal conductivity in diamondoid lattices: high thermoelectric performance in chalcopyrite $Cu_{0.8+y}Ag_{0.2}In_{1-y}Te_2$

Hongyao Xie[1], Shiqiang Hao[2], Songting Cai[2], Trevor P. Bailey[3], Ctirad Uher[3], Christopher Wolverton[2], Vinayak P. Dravid[2], and Mercouri G. Kanatzidis[1*]

[1]Department of Chemistry, Northwestern University, Evanston, Illinois 60208, USA.

[2]Department of Materials Science and Engineering, Northwestern University, Evanston, Illinois 60208, USA.

[3]Department of Physics, University of Michigan, Ann Arbor, Michigan 48109, USA.
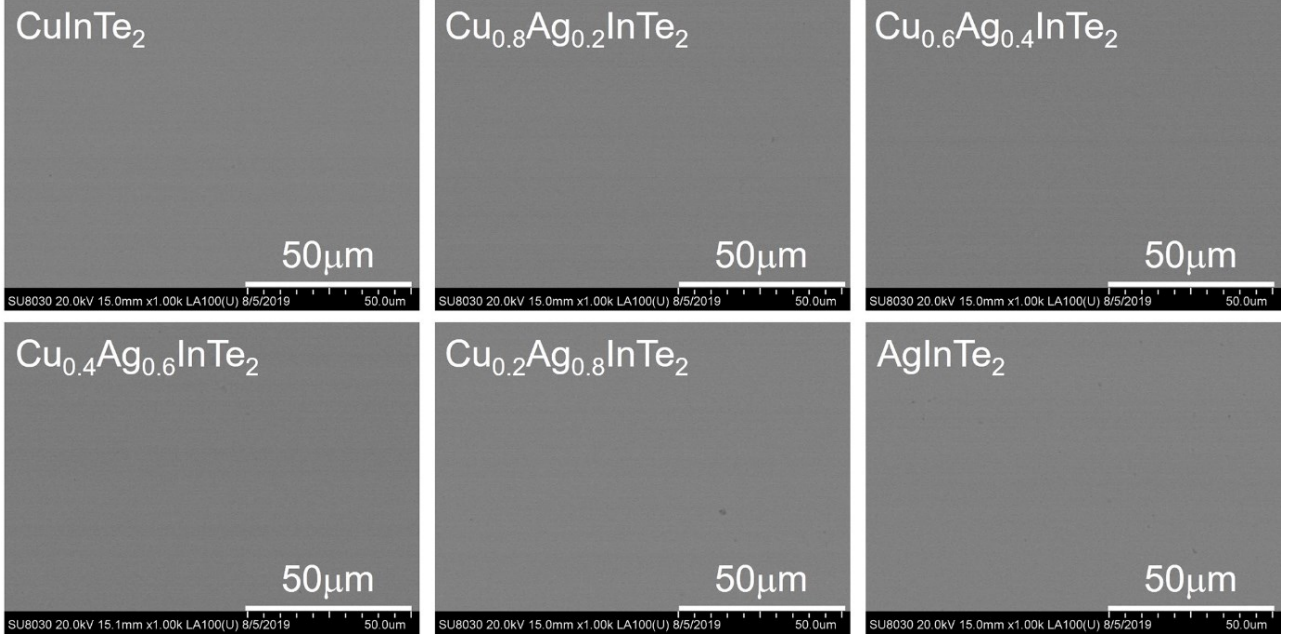
1. Microstructure.

Figure S1. BSE images of the polished surfaces of SPS-sintered $Cu_{1-x}Ag_xInTe_2$ (x = 0, 0.2, 0.4, 0.6, 0.8 and 1) compounds, demonstrating the lack of impurity phases on the micron scale in all samples.

2. Lattice thermal conductivity calculation.

We estimated the lattice thermal conductivity simply by subtracting the electronic thermal conductivity from the measured total thermal conductivity[1]:

$$\kappa_L = \kappa - \kappa_e = \kappa - L\sigma T \tag{S1}$$

where κ_L, κ and κ_e are the lattice thermal conductivity, total thermal conductivity and electronic thermal conductivity, respectively. The latter can be estimated by the Wiedemann-Franz relation: $\kappa_e = L\sigma T$, where σ is the electrical conductivity and L is the Lorenz number. Assuming a single parabolic band model, the Lorenz number L is calculated from[2, 32-3]:

$$L = \left(\frac{k_B}{e}\right)^2 \left(\frac{(r+7/2)F_{r+5/2}(\eta)}{(r+3/2)F_{r+1/2}(\eta)} - \left[\frac{(r+5/2)F_{r+3/2}(\eta)}{(r+3/2)F_{r+1/2}(\eta)} \right]^2 \right) \tag{S2}$$

Here, the reduced Fermi energy η can be obtained from the Seebeck coefficient as:

$$\alpha = \frac{k_B}{e}\left(\frac{(r+5/2)F_{r+3/2}(\eta)}{(r+3/2)F_{r+1/2}(\eta)} - \eta \right) \tag{S3}$$

with the Fermi integral defined as:

$$F_n(\eta) = \int_0^\infty \frac{\chi^n}{1 + e^{\chi - \eta}} d\chi \qquad (S4)$$

where k_B is the Boltzmann constant, e is the electron charge, α is the Seebeck coefficient and r is the scattering factor; here $r = -1/2$ is appropriate for acoustic phonon scattering. Thus, the lattice thermal conductivity can be obtained.

3. Low temperature carrier concentration and carrier mobility.

The low temperature (10-300 K) carrier concentration and carrier mobility are shown in **Figure S2**. The carrier concentration and carrier mobility dramatically decrease with increasing Ag content, reflecting the poor conductive nature of $AgInTe_2$. The carrier concentration is nearly independent of temperature in all samples. For pristine $CuInTe_2$, the carrier mobility follows the $T^{3/2}$ dependence in the temperature range of 10–100 K, indicative of ionized impurities dominating the charge carrier scattering. However, above 200 K, the temperature dependence changes to the $T^{-1/2}$ variation, which suggests that the dominant carrier scattering process is alloy scattering.
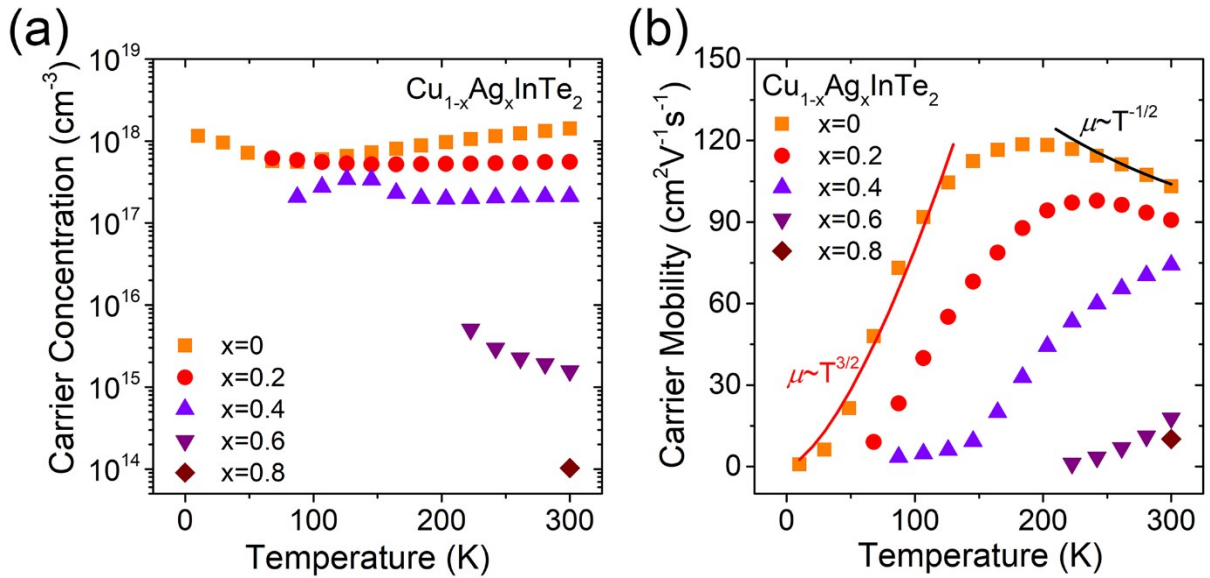

Figure S2. Temperature dependence of (a) carrier concentration and (b) carrier mobility for $Cu_{1-x}Ag_xInTe_2$ (x = 0, 0.2, 0.4, 0.6, 0.8 and 1).

4. Thermal conductivity.

The calculated Grüneisen parameters for $CuInTe_2$, $AgInTe_2$ and $Cu_{0.5}Ag_{0.5}InTe_2$ are shown in **Figure S3**. The absolute values of the Grüneisen parameters increase with increasing Ag content, suggesting larger anharmonicity and thus lower lattice thermal conductivity. The

theoretically calculated lattice thermal conductivities indicate the Ag is effective in decreasing the lattice thermal conductivity of $Cu_{1-x}Ag_xInTe_2$, consistent with the experimental results.
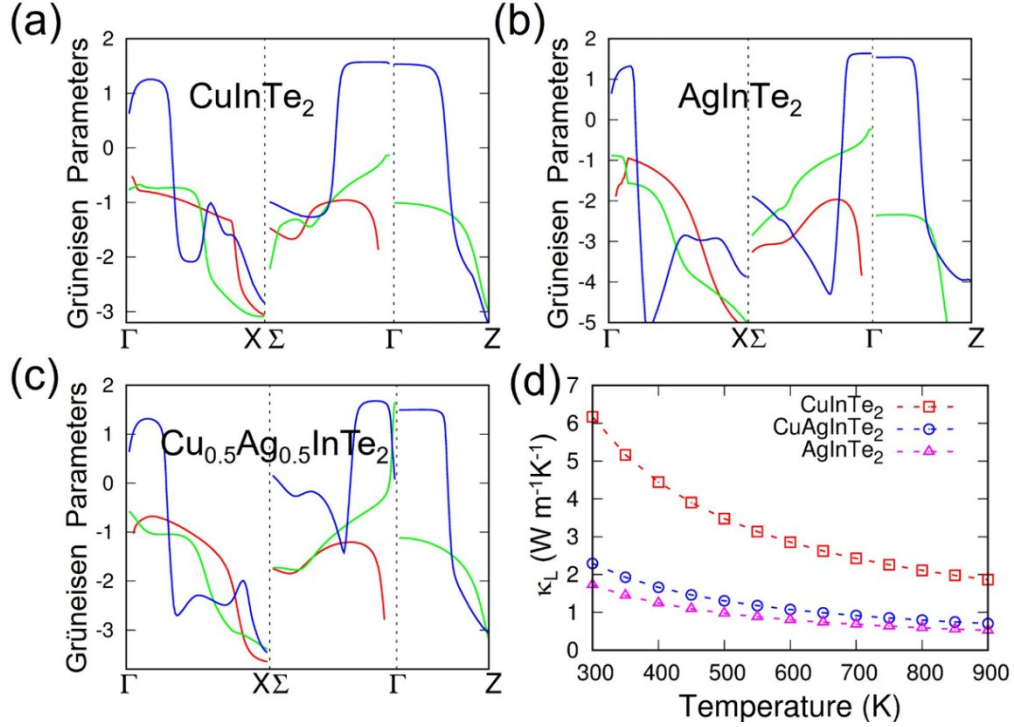

Figure S3 Calculated Grüneisen parameters for (a) $CuInTe_2$, (b) $AgInTe_2$, and (c) $Cu_{0.5}Ag_{0.5}InTe_2$; (d) theoretically calculated lattice thermal conductivities of $CuInTe_2$, $AgInTe_2$ and $Cu_{0.5}Ag_{0.5}InTe_2$.

Table S1. Parameters obtained by fitting the experimental lattice thermal conductivity data to the Debye-Callaway model (Eq. 2 of the main text) for $Cu_{0.8}Ag_{0.2}InTe_2$. Here, v/L is the inverse relaxation time for grain boundary scattering, A and B are the constants for point defect scattering and phonon-phonon scattering, respectively, and C_1 and C_2 are the constants for phonon resonance scattering.

Sample	v/L ($10^7 s^{-1}$)	A ($10^{-42} s^3$)	B (10^{-18} s/K)	C_1 ($10^{35} s^{-3}$)	C_2 ($10^{35} s^{-3}$)
$Cu_{0.8}Ag_{0.2}InTe_2$	6.65	3.638	7.323	3.062	3.589

5. Phonon mean free path and Grüneisen parameter calculation.

It is well known that the lattice thermal conductivity for a solid can be described as[4]:

$$\kappa_L = \frac{1}{3}C_v v_{ave} l_{ph} \tag{S5}$$

where C_v is the heat capacity, v_{ave} is the average sound velocity, and l_{ph} is the phonon mean free path. The average sound velocity is given as[5]:

$$v_a = \left[\frac{1}{3}\left(\frac{1}{v_l^3}+\frac{2}{v_s^3}\right)\right]^{-1/3} \tag{S6}$$

where v_l is the longitudinal sound velocity and v_s is the shear sound velocity. Thus, the phonon mean free path can be obtained by using the measured thermal conductivity, sound velocity and heat capacity data.

The Grüneisen parameter γ_G can be calculated by the following relationships[6, 7]:

$$\gamma_G = \frac{3}{2}\left(\frac{1+v_p}{2-3v_p}\right) \tag{S7}$$

$$v_p = \frac{1-2(v_s/v_l)^2}{2-2(v_s/v_l)^2} \tag{S8}$$

6. Phase structure, optical absorption spectra and carrier concentration for $Cu_{0.8+y}Ag_{0.2}In_{1-y}Te_2$ compounds.

The XRD patterns for all sintered $Cu_{0.8+y}Ag_{0.2}In_{1-y}Te_2$ compounds can be indexed to the chalcopyrite structure, except one tiny impurity peak around $27.6°$ was observed when $y \geq 0.05$, and the XRD peaks of all samples shift to higher angle with the smaller Cu substituting into the In site, as shown in **Figure S4**.
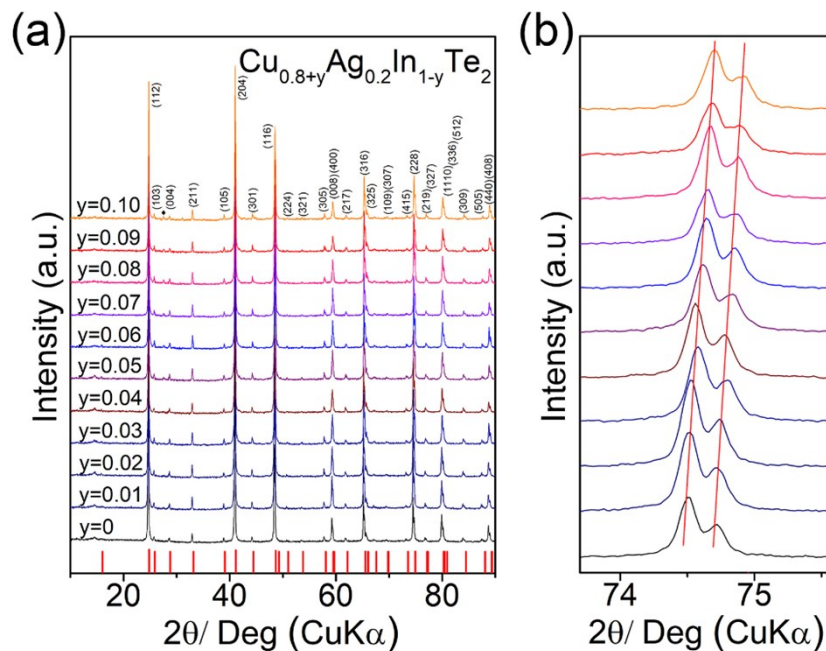

Figure S4. (a) XRD patterns of SPS-sintered $Cu_{0.8+y}Ag_{0.2}In_{1-y}Te_2$ (y = 0, 0.01, 0.02, 0.03,

0.04, 0.05, 0.06, 0.07, 0.08, 0.09 and 0.10), the indices of crystal planes for $CuInTe_2$ as shown in figure. (b) An enlarged figure for the high angle XRD peak, with all peaks shifting to higher angles with increasing Cu content, indicating a successful entry of Cu on the sites of In in the chalcopyrite structure.

Figure S5 depicts the optical absorption spectra of $Cu_{0.8+x}Ag_{0.2}In_{1-x}Te_2$. The electronic energy band gaps for all samples are close to 0.9 eV, indicating Cu doping does not change the band gap of the compound. The small absorption observed at ~0.64 eV for all samples corresponds to the characteristic absorption of water.
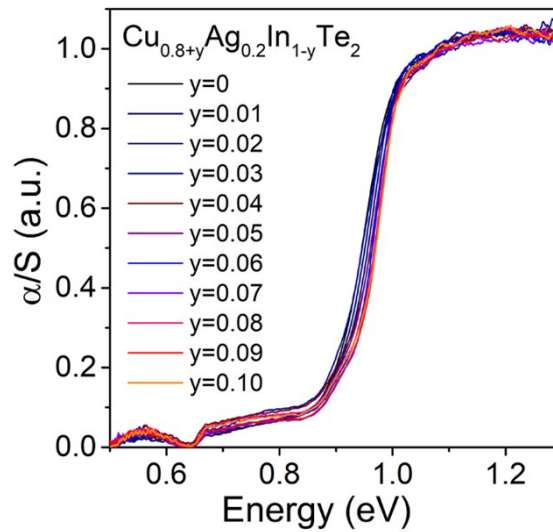

Figure S5. Optical absorption spectra of $Cu_{0.8+y}Ag_{0.2}In_{1-y}Te_2$ compounds.

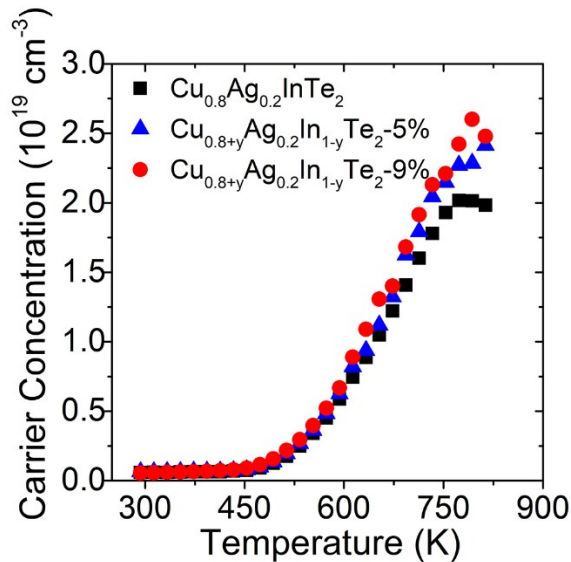Figure S6. The temperature dependence of carrier concentration in linear coordinate for $Cu_{0.8}Ag_{0.2}InTe_2$, $Cu_{0.85}Ag_{0.2}In_{0.95}Te_2$ (5%Cu) and $Cu_{0.89}Ag_{0.2}In_{0.91}Te_2$ (9%Cu).

7. Carrier mean free path calculation.

The carrier mean free path was calculated by assuming the dominance of acoustic phonon scattering[8]:

$$l_0 = \frac{3\mu(2\pi m^* kT)^{1/2}}{4e} \tag{S9}$$

where m^* is the carrier effective mass, μ is the carrier mobility, k is the Boltzmann constant and e is the electron charge.

Reference:

1.   G. J. Snyder and E. S. Toberer, *Nat Mater*, 2008, **7**, 105-114.
2.   L. D. Zhao, S. H. Lo, J. He, H. Li, K. Biswas, J. Androulakis, C. I. Wu, T. P. Hogan, D. Y. Chung, V. P. Dravid and M. G. Kanatzidis, *J. Am. Chem. Soc.*, 2011, **133**, 20476-20487.
3.   W.-S. Liu, Q. Zhang, Y. Lan, S. Chen, X. Yan, Q. Zhang, H. Wang, D. Wang, G. Chen and Z. Ren, *Adv. Energy Mater.*, 2011, **1**, 577-587.
4.   T. M. Tritt, *Thermal conductivity: theory, properties, and applications*, Springer Science & Business Media, 2005.
5.   T. J. Zhu, S. N. Zhang, S. H. Yang and X. B. Zhao, *Phys. Status Solidi RRL*, 2010, **4**, 317-319.
6.   Y. Pei, C. Chang, Z. Wang, M. Yin, M. Wu, G. Tan, H. Wu, Y. Chen, L. Zheng, S. Gong, T. Zhu, X. Zhao, L. Huang, J. He, M. G. Kanatzidis and L. D. Zhao, *J. Am. Chem. Soc.*, 2016, **138**, 16364-16371.
7.   D. S. Sanditov and V. N. Belomestnykh, *Tech. Phys.*, 2011, **56**, 1619-1623.
8.   Y. Zheng, Q. Zhang, X. Su, H. Xie, S. Shu, T. Chen, G. Tan, Y. Yan, X. Tang, C. Uher and G. J. Snyder, *Adv. Energy Mater.*, 2015, **5**, 1401391.